



## Formation of an Au membrane incorporated with carbon atoms under electron beam irradiations



Seong Soo Choi<sup>a,\*</sup>, Myoung Jin Park<sup>a</sup>, Chul Hee Han<sup>a</sup>, Sae-Joong Oh<sup>a</sup>, Tokutaro Yamaguchi<sup>a</sup>, Nam Kyou Park<sup>b</sup>, Jung Ho Yoo<sup>c</sup>, Kyoung Jin Park<sup>c</sup>, Yong-Sang Kim<sup>d</sup>

<sup>a</sup> Research Center for Nanobio Science, SunMoon University, Ahsan, Chungnam 31460, Republic of Korea

<sup>b</sup> School of Electrical Engineering, Seoul National University, Seoul 08826, Republic of Korea

<sup>c</sup> Team for Measurement and Analysis, National Nano-Fabrication Center, Daejeon 34141, Republic of Korea

<sup>d</sup> School of Electronic and Electrical Engineering, Sungkyunkwan University, Suwon 16419, Republic of Korea

### ARTICLE INFO

#### Article history:

Received 26 December 2015

Revised 5 May 2016

Accepted in revised form 12 May 2016

Available online 17 May 2016

#### Keywords:

Nanopore on pyramid

Electron beam irradiation

Surface tension

EDAX (Energy Dispersive X-ray Analysis)

Au cluster

Ostwald ripening

### ABSTRACT

The Au nanopore can be utilized as optical nano-bio sensor due to its plasmonic effect. Initially, we fabricated the pore membrane inside the focused ion beam drilled Au apertures by using various electron beam irradiations. Depending upon the electron beam current density, the pore closing and opening phenomena of the diffused membrane were examined and characterized by electron probe micro analysis (EPMA), transmission electron microscopy (TEM), and energy-dispersive X-ray analysis (EDAX). No Au atoms were observed right after electron beam irradiations due to the low Au atomic concentrations below the detection limit of TEM. However, after the samples were kept under a laboratory environment for one year, several Au clusters with a size of 5 nm–7 nm were formed on the diffused membrane. This phenomenon can be attributed to Ostwald ripening.

© 2016 Elsevier B.V. All rights reserved.

### 1. Introduction

There have been many studies related to fabrication of the solid state nanopore using various techniques such as ion sculpting, high energy electrons beams due to the possible ultrafast genome sensing capabilities of the nanopore [1,2]. The solid-state nanopores with SiN<sub>3</sub> or SiO<sub>2</sub> with an electrical detection technique have been successfully fabricated by using electron beam irradiation techniques such as field emission scanning microscopy (FESEM) and transmission electron microscopy (TEM) [3–5]. However, the recent portable nanopore device with an electrical detection technique manufactured by Oxford Nanopore Company is reported to present high error rates [6–8]. In addition, the current genome sequencing is performed under the optical detection technique, and the plasmonic nanochannel devices are currently utilized as optical biosensors [9–10]. The Au optical nanopore has yet to be fabricated. Fabrication of nanopore on pyramid by diffusion of Au and carbon under electron beam irradiations was reported previously [11,12]. In this report, we present the Au nanoparticle or cluster formation in the diffused pore-membrane on the FIB drilled Au aperture by using electron beam irradiations.

Influence of electron beam irradiation on the pore formation depends upon the electron instruments such as TEM and FESEM. When the electron beam is irradiated on the specimen using TEM, depending upon the ratio of membrane thickness to the aperture diameter, the nanometer size hole will either shrink or become open [1]. This phenomenon is attributed to the surface tension on the membrane, which become viscous from electron beam irradiations. Resizing of hole on the viscous fluid membrane or on the heated metallic membrane is well documented before [13,14]. However, under electron beam irradiations using FESEM, the hole always shrinks, regardless of the ratio of membrane thickness to the hole diameter [3–5]. For accelerating energy less than 5 kV of FESEM, most of electron energy will be deposited in the ~10<sup>2</sup> nm thick specimen due to the shallow penetration depth of electron less than 50 nm [15]. Temperature rise of the specimen under FESEM electron beam irradiation will depend on the thermal conductivity of the specimen, deposited electron energy, and the Au particle size in the sample. Pore formation under a FESEM electron beam irradiation would rather depend on the concentration dependent diffusion in the solid-state, rather than on the surface. However, this phenomenon is still under investigation.

Electron beam induced melting and local temperature rise by using electron probe micro-analysis (EPMA) have been reported by Casting and et al. [16,17]. Electron beam irradiation on the sample surface would provide the surface diffusion for nanopore formation on the

\* Corresponding author at: RM2408, Research Center for Nanobio Science, College of Natural Science, SunMoon University, Ahsans, Chungnam 31460, Republic of Korea.

E-mail address: [sscphy2010@gmail.com](mailto:sscphy2010@gmail.com) (S.S. Choi).

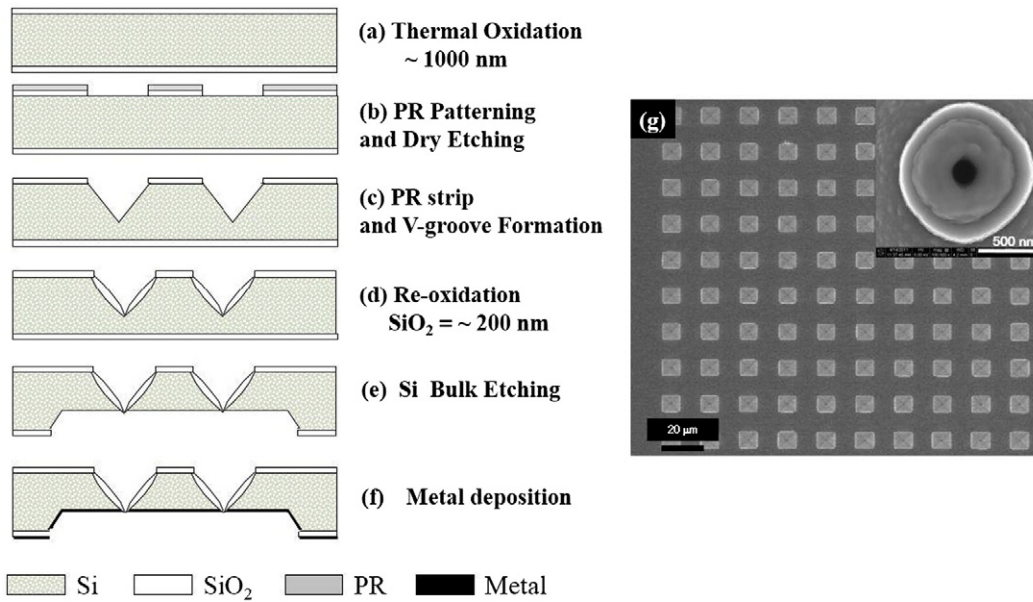


**Fig. 1.** Schematic drawing for microfabrication process. Thermal oxidation in (a) followed by photoresist patterning and dry etching (b), V-groove formation (c), re-oxidation (d), backside Si bulk etching (e) were followed. After nano-aperture opening (e), a 200 nm Au film was deposited by using a DC 400 W electron beam sputter (f), and a FESEM image for a  $(10 \times 10)$  pyramidal array with an aperture on the apex (top right) is shown in (g).

nanometer thick membrane. The surface tension force, along with the high vapor pressure of the material in the vacuum condition ( $10^{-7}$  Torr– $10^{-8}$  Torr), will become factors to pore formation during electron beam irradiation by using FESEM and TEM. The melting temperature of the bulk gold is 1337 K. Depending upon the viscosity of the heated membrane, the surface tension force, and the vapor pressure of the material, the pore widening and the shrinking are expected to occur. In addition, Monte Carlo simulation results show that nanoscale local temperature rise is high enough to make the Au films melt and evaporate during electron beam irradiations even at low accelerating voltage of (1–30 kV) [17]. During high energy TEM electron beam irradiations with accelerating voltages of  $\sim 200$  kV, the nanoscale local temperature rise by inelastic collisions; Coulomb explosion of electrons, electron beam induced thermal spike, nano-particle melting, and vaporization depending upon the particle size were also reported [18–26]. For electron energy of  $\sim 10^2$  keV of TEM, most of energy will be transmitted and the local temperature rise would depend on inelastic collisions; Coulomb explosion and thermal spikes. Charging effects from insufficient contacts with specimen supports during electron beam irradiations also present melting temperature change [19], and the melting temperature dependent upon the size of the particles and clusters is also reported [25–27].

During electron beam irradiation on the specimen, the hydrocarbon contamination has been a problem for fabrication of the metallic nanopore [28,29]. When electron beam is irradiated over the micrometer size area, the annular contamination will be formed with higher

carbon contamination buildup at the periphery of the irradiated area than at the center. This stems from the surface diffusion of the absorbed hydrocarbon on the specimen toward the center of the irradiation area. The diffused hydrocarbons will be cross-linked to the surface during electron beam irradiations on the surface. Hence carbon contamination ring will be formed and it will be difficult for carbon atoms to diffuse into the center of the irradiating area [30,31].

In addition, the low nuclear mass of hydrogen results in a threshold energy for displacement energy below 2 keV. The C–H bond energy is 4.36 eV and its corresponding displacement energy is very low compared with other some organic compounds [28]. Hence, during electron beam irradiations, hydrogen atoms will be knocked out by electron bombardments, and the mobile surface hydrocarbon deposits are converted into amorphous carbons. The resulting amorphous carbon adsorbates are cross-linked to the surface and become stable under further electron irradiations.

Carbon encapsulation of Au atoms under heating and Au evaporation during TEM imaging are also examined [32,33]. When gold atoms are covered by carbon atoms, the Au atoms become more stable with carbon atoms than without carbon atoms [34]. In addition, Au clusters smaller than 1 nm in diameter cannot be resolved due to detection limit and low contrast on the amorphous substrate by TEM. However, when the samples were kept for 4 months under room temperature environments, Au cluster formation and island formation on the amorphous films is observed [34]. This phenomenon is attributed to Ostwald ripening process; large particles are thermodynamically more favorable

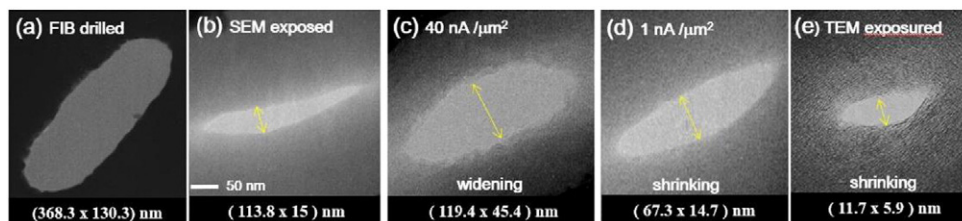


**Fig. 2.** A TEM image of a FIB drilled Au slit-type nano-aperture is shown in (a). After a SEM exposure at 20 keV, the pore of  $(113.8 \text{ nm} \times 15.0 \text{ nm})$  size on the diffused membrane is presented in (b). Then, after 100 s electron exposure with  $40 \text{ nA}/\mu\text{m}^2$  electron beam currents density using EPMA, the nanopore is widened to  $(119.4 \text{ nm} \times 45.4 \text{ nm})$  in (c). However, for an electron beam exposure with  $1 \text{ nA}/\mu\text{m}^2$  beam current density, the pore was shrunk to  $(67.3 \text{ nm} \times 14.7 \text{ nm})$  in (d). After a TEM electron exposure at 200 keV, the pore was shrunk again to  $(11.7 \text{ nm} \times 5.9 \text{ nm})$  in (e).

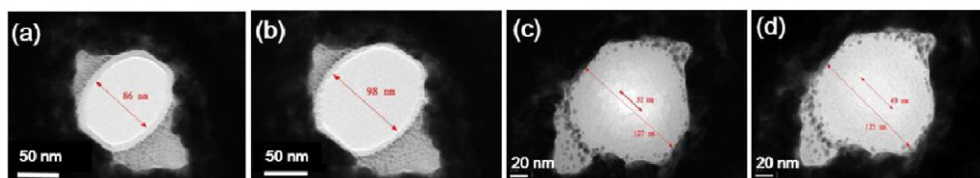


**Fig. 3.** TEM images of the Au nano-apertures are presented after FIB drilling (a), after 100 pA, 300 keV TEM electron beam irradiation for 50 min (b), 1.5 keV FESEM electron beam irradiation for 10 min (c), and 100 pA, 300 keV TEM electron beam irradiation for 40 min (d). No shape change is shown after a 100 pA electron beam irradiation in (b). However, after 1.5 keV FESEM electron beam irradiation, a diffused membrane was formed, and the diffused membrane became thinner and the pore became widened after another 100 pA electron beam irradiation at 300 keV by using TEM.

than small particles [35]. Hence, small particles has tendency to condense on the larger particles. Therefore, all the small particles will shrink and larger particles will become larger. In this report, nanopore formation, shrinking and opening of the electron beam induced membrane, and the Au cluster formation process on the diffused membrane will be presented.

## 2. Experimental process and its results

### 2.1. Fabrication process of pyramidal array

The pyramidal nanometer size apertures on top of the oxide pyramid array were fabricated using conventional Si microfabrication techniques. The (10 × 10) micrometer patterns were engraved using such as photolithography followed by tetramethylammonium hydroxide (TMAH) alkaline wet etching, stress-induced thermal oxidation below 1000 °C, and a backside bulk Si etching process for oxide pyramidal revealing. Then, a two step metal sputter deposition process was followed by using a DC 400 W electron beam sputter. Then, plasma dry etching of the supporting SiO<sub>2</sub> layer was performed to reveal the free standing Au membrane only. Fig. 1 presents the detailed fabrication process for the pyramidal array.

### 2.2. Various electron beam irradiation on the drilled Au aperture

After the Au apertures were drilled by 30 keV Ga ion focused ion beam (FIB), the various electron beam irradiations were carried out in order to reduce the aperture diameter down to a-10<sup>0</sup> nm nanometer. Electron beam irradiation techniques such as TEM (JEM-2010 and JEM-3011 HR.), FESEM (JSM 6400), and electron probe micro-analysis (EPMA, JSA-8100) were utilized. TEM can provide high electron voltages ranging from 100 keV to 300 kV and the currents with ~order of 100 pA, and EPMA can offer the adjustable probe diameter and currents with electron voltage range of (1–30) kV.

First, we carried out the resizing experiments dependent upon the electron beam current density using EPMA. EPMA can provide the adjustable probe beam diameters ranging from micrometer to nanometer. Fig. 2 presents the widening and the shrinking phenomena of the slit-type aperture depending upon the electron beam current density. The long slit-type hole with 368.3 nm length and 130.3 nm width was drilled on top of the pyramidal structure by using a 30 keV Ga ion focused ion beam technique (Dual-Beam Helio NanoLab). Then, a 5-minute electron beam irradiation at 5 kV was carried out by using FESEM to reduce the size of the drilled hole down to (113.8 nm × 15.0 nm). A 100-second electron beam irradiation (with electron projection diameter of 4 μm) was followed with a probe beam current density of 40 nA/μm<sup>2</sup>, and a probe diameter of 4 μm by using 20 keV EPMA. Then, the nanopore size was slightly opened to (119.4 nm × 45.4 nm) in Fig. 2(c). However, under an electron beam irradiation with a probe electron beam current density of 1 nA/μm<sup>2</sup> with same probe diameter of 4 μm. The pore was shrunken down to (67.3 nm × 14.7 nm) in Fig. 2(c). Finally, the pore was shrunken down to (11.7 nm × 5.9 nm) size under 300 keV TEM electron beam irradiation at 1 pA. After each electron beam irradiation by using EPMA, the sample was taken out from the EPMA chamber and was inserted into the TEM chamber for TEM imaging.

Fig. 3 presents the TEM images of the FIB drilled Au aperture under electron beam treatments by using FESEM and TEM. During FIB milling of a 200 nm thick Au film, the small Au clusters on the grey-colored membrane on the periphery of the ~86 nm wide Au aperture were shown in Fig. 3(a). These Au clusters on the diffused membrane are formed due to thermal spike during 30 keV Ga ion beam milling. Then, we carried out a 50-minute electron beam irradiation at 300 keV with a 100 pA beam current, however, shrinking of the aperture was not observed, only to make the diffused membrane around the periphery of the drilled Au aperture evaporated in Fig. 3(b). However, for a 1.5 keV FESEM electron beam irradiation for 10 min, a 32 nm wide nano-opening area on the diffused membrane was formed as in Fig. 3(c). Then, again, under a 300 keV TEM electron beam irradiation with

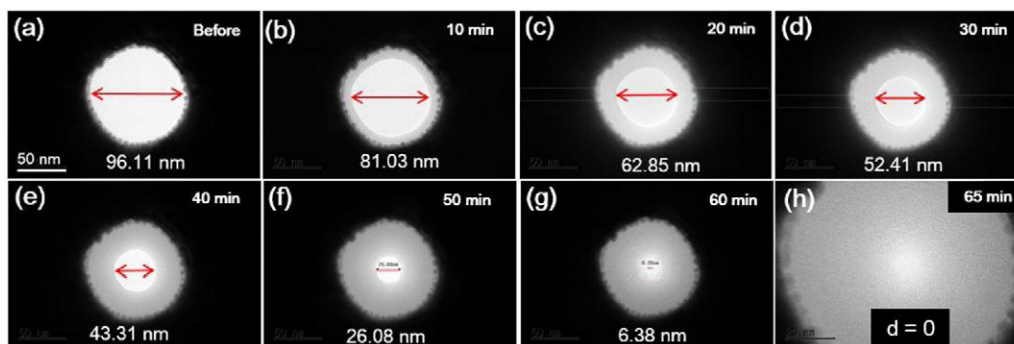


**Fig. 4.** The TEM images of a FIB drilled Au aperture reduction after successive electron beam irradiations are shown. Reduction of a nano-aperture from 96.11 nm in diameter to 81.03 nm is shown after first 300 keV TEM electron beam irradiation with a beam current of 1 pA for 10 min in (b). After successive 60 min irradiations, the aperture area was reduced to 6.38 nm in (g). The reduction rate is measured to be 1.50 nm/min. After a 65 min irradiation time, the aperture was completely closed.

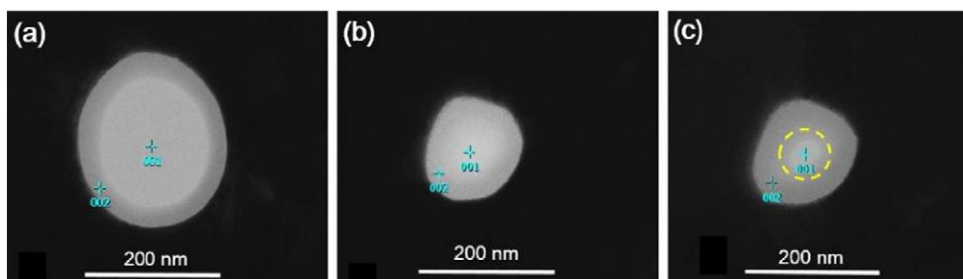


**Fig. 5.** TEM images for EDAX point analysis are shown. The image (c) is taken after EDAX analysis on the sample (b) is performed. The center area is damaged and become evaporated due to an intense 2.5 nA probe current density.

100 pA for 40 min, the pore on the diffused membrane was widened to 49 nm as in Fig. 3(d). The entire dark grey membrane area became a bright-grey colored area after a TEM electron beam exposure. This indicates that the diffused membrane becomes thinner during a 300 keV electron beam irradiation, due to evaporation of the membrane atoms.

Fig. 4 shows the successive TEM images with 10 min intervals. The electron beam irradiations at 300 keV with 0.5 pA were performed on the sample with identification number (S11# 4-10-2 B) by using TEM (HR JEM-3011). The pore diameter on the diffused membrane was reduced from 96.11 nm to 81.03 nm after a 10 min irradiation in Fig. 4(a) and (b). Final diameter of the pore on the diffused membrane is shown to be 6.38 nm, after total 60 min of successive irradiations in Fig. 4(g). The average shrinking rate is measured to be 1.5 nm/min. After 65 min of irradiations, the pore on the diffused membrane was completely closed in Fig. 4(h).

### 2.3. Chemical analysis of the diffused membrane by EDAX

The chemical analysis for the electron beam induced membrane was also performed by using an EDAX system with scanning TEM (STEM, JEOL 2100F). The EDAX analysis using 200 keV STEM can provide a better qualitative result than EDAX analysis using FESEM due to a larger and better detector system at 200 keV STEM. The focused electron beam probe with a 1.5 nm diameter is set to 2.5 nA probe current at 200 keV and 40 s of duration time. Three different samples irradiated by FESEM electron beam are prepared for EDAX analysis in Fig. 5. Table 1 presents the ratios of Au atoms to C atoms on the different spots on each sample. Three different points are selected; a center point on the diffused area, a peripheral point on the diffused area, a third point on the 200 nm Au bulk area. The Au atomic percent at the center area for sample (a) and sample (b) is 15.31% and 2.82%, respectively. The ratios of Au atomic

percent to carbon atomic percent for the diffused grey areas for sample (a), (b), and (c) are ~0.12, 0.09, and 0.09, respectively. However, the ratios of the Au atomic percent to the carbon atomic percent on the 200 nm Au bulk area for (a), (b), and (c) are 2.2, 2.48, and 2.15, respectively. During EDAX point analysis on the center in the sample (b), the center region is damaged and the void area with a 30.4 nm diameter is presented as in Fig. 5(c). This can be due to “electron beam induced evaporation” due to very intense 2.5 nA probe currents with a 1.5 nm probe diameter. The beam shifting due to an unstable electron beam irradiation can be attributed to the large evaporated area of 30.4 nm width. These data present the followings; (i) the diffused membrane contains both gold and carbon atoms. (ii) At the center, the ratio of the Au atom concentration to the carbon atom concentration is highest; the richest Au atom concentration at the center, (iii) carbon contamination ring: The highest carbon concentration in the peripheral region than any other points is observed.

### 2.4. Au cluster formation on the diffused membrane

TEM images after electron beam irradiations by using 200 keV TEM are presented in Fig. 6. Initially, no particles or clusters on the diffused membrane are observed, right after electron beam irradiation by using FESEM or TEM. However, after the sample was kept in a desiccator for 1 year under a room environment, we observed several Au clusters (red circled) formed on the diffused membrane in (b). The shape of the large opening was changed and the small void opening was completely closed. The formation of the Au clusters can be attributed to Ostwald ripening effect; the larger particles would become larger and larger from the expense of smaller particles in order to minimize the system surface energy. The Au atoms below the TEM detection limit (~1 nm) are not able to detect, or it is impossible to obtain the Au particle [31]. In addition, the Au (1 × 1) surface on the amorphous carbon (a-c) membrane does exhibit more stable than the Au (1 × 1) surface without carbon membrane [33]. Au atoms diffuse together with carbon atoms under electron beam irradiations, and Au nanoparticles coalesce into clusters or larger particles via Ostwald ripening on the a-C membrane under a room environment [33–35]. The Au particle with a 2.3 nm lattice spacing for 10 atomic rows is shown in Fig. 6(c). The influence on the Au cluster formation on the electron beam irradiation is still under investigation.

## 3. Results and discussion

We address the following experimental results;

- (i) Depending upon the electron beam current density, the shrinking or opening of the slit-type aperture on the pyramidal apex was observed by using EPMA. The higher electron beam currents will present the higher temperature rise on the local specimen area beyond the evaporation temperature. The melting of the local specimen area and evaporation of the atoms would influence the pore opening and shrinking.

**Table 1**

The ratios of gold atom to carbon atom in the sample are given as below. Among three sampling areas of the center of the membrane, of the dark grey peripheral area, and the dark Au bulk area, the Au concentrations at the center are measured to be the highest and the lowest on the peripheral area. The evaporated area on the center of the diffused membrane in (c) is not available due to electron beam damage for EDAX analysis (written in red colored letter).

		Ratio (Au/C)		
		Center (001)	Grey membrane (002)	200 nm thick Au (black area)
Sample a (big circle)	Atomic %	15.31	0.12	2.2
	Mass %	249	2.01	37.51
Sample b (small circle closed)	Atomic %	2.82	0.092	2.48
	Mass %	46.08	1.46	40.7
Sample c (after EDS, pore damaged)	Atomic %	N/A	0.09	2.15
	Mass %	N/A	1.43	35.25

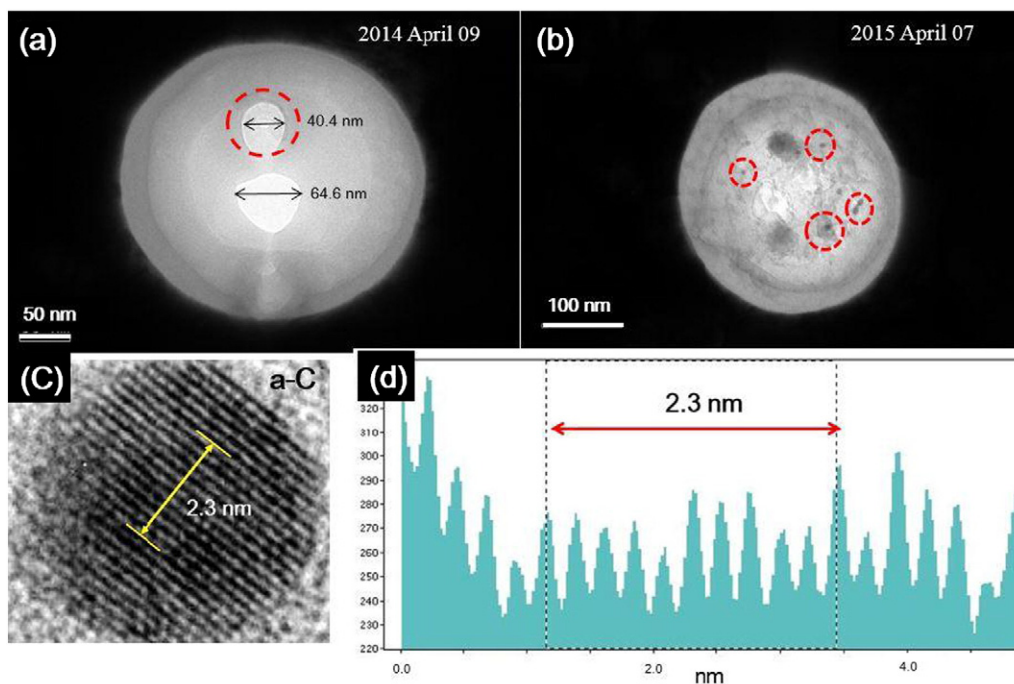


**Fig. 6.** A TEM image of the nano-membrane after several electron beam irradiations in the FIB drilled Au nano-aperture is shown in (a). No Au particles are shown. After 1 year later, the Au particles and clusters are shown in the diffused membrane in (b). The Au particle with its atomic spacing of 2.3 nm for 10 atomic rows is presented.

- (ii) Pore opening and shrinking dependent upon the electron beam current density; for electron irradiations on the specimen by using TEM, pore opening and shrinking are observed. For  $\sim 1$  pA electron beam current irradiation, the Au and carbon atomic diffusion occurs. We successfully controlled pore (opening) with its shrinking rate of 1.5 nm/min with 0.5 pA. However, for 100 pA electron beam current, we did not observe any change of aperture shape. This phenomenon can be attributed to evaporation of atoms arising from the temperature rise on the nano-scale irradiation area. The temperature rise from the electron beam induced thermal spike during 100 pA electron beam irradiation at 300 kV can be as high as the evaporation temperature of Au particles. Under a proper electron beam dose of  $\sim 1$  pA or below, the temperature rise would make the Au specimen surface viscous. Then, the surface energy in the viscous membrane would make the hole either shrink or open depending upon the ratio of the membrane thickness to the pore diameter.

However, under 1.5 kV FESEM electron beam irradiations with the scanning area ( $\sim 1 \mu\text{m} \times 1 \mu\text{m}$ ) and 1.4 nA probe current, the diffused membranes were always formed. The local temperature rise can be very high enough to present the solid-state atomic diffusion. The detailed physical mechanism behind these phenomena is still under investigation.

- (iii) Electron beam induced evaporation and formation of carbon contamination ring; we also observed the highest Au atomic concentrations on the center of the diffused membrane, and the carbon contamination ring at the periphery of the diffused membrane. During EDAX analysis with a 1.5 nm probe diameter and an intense beam current of 2.5 nA at 200 keV, a  $\sim 30$  nm wide area on the center area of the diffused membrane was evaporated. Due to unstable beam positioning during irradiation, the evaporated area became wide up to  $\sim 30$  nm.
- (iv) Au particle or cluster formation on the diffused membrane; we observed an Au cluster formation on the electron beam induced membrane after being kept under the room environment for

1 year. These phenomena can be attributed to Ostwald ripening process; the larger particles are thermodynamically more stable than the smaller particles.

#### 4. Conclusion

The nano-pore on the diffused membrane can be controlled by using proper electron beam irradiation conditions, and the formation of the Au particles on the diffused membrane was observed under the room environments. The optimization for Au nano-particle formation is still under investigation. With proper pore opening and the Au particle formation on the pore membrane, the fabricated nanopore inside the FIB-drilled Au aperture can be an excellent candidate for single molecule bio sensor device.

#### Acknowledgements

This work was partially supported by the Basic Science Research Program through the National Research Foundation (Nanopatterned Optical Nanopore for Single Molecule Manipulation and Analysis, NRF 2015-R1D1A1A-09056781) and by Global Research Laboratory funding (GRL; Nanoplasmonic Integrated Circuits for Ultrafast Information Processing, KRF Grant No. K2081500003-2008-00580).

#### References

- [1] A.J. Storm, J.H. Chen, X.S. Ling, H.W. Zanbergen, C. Dekker, *Nat. Mater.* 2 (2003) 537–540.
- [2] J. Li, Stein, C. McMullan, D. Branton, M.J. Aziz, J.A. Golovchenko, *Nature* 412 (2001) 166–169.
- [3] A.S. Prabhu, K.J. Freedman, J.W.F. Robertson, Z. Nikolov, J.J. Kasianowicz, M.J. Kim, *Nanotechnology* 22 (2011) 425302.
- [4] H. Chang, S.M. Iqbal, E.A. Stach, A.H. King, N.J. Zaluzec, R. Bashir, *Appl. Phys. Lett.* 88 (2006) 103109.
- [5] C.J. Lo, T. Aref, A. Bezryadin, *Nanotechnology* 17 (2006) 3264–3267.
- [6] A. Mikheyev, M.M.Y. Tin, *Mol. Ecol. Resour.* 14 (2014) 1097–1102.
- [7] E.C. Hayden, *Nat. News* (February 14 2014), <http://dx.doi.org/10.1038/nature.2014.14724>.
- [8] E.C. Hayden, *Nature* 521 (2015) 15–16.

- [9] F. Eftekhari, C. Escobedo, J. Ferreira, X. Duan, E.M. Girotto, A.G. Broto, R. Gordon, D. Sinton, *Anal. Chem.* 81 (2009) 4308–4311.
- [10] M.P. Jonsson, A.B. Dahlin, L. Feuz, S. Petronis, F. Hook, *Anal. Chem.* 82 (2010) 2087–2094.
- [11] S.S. Choi, M.J. Park, T. Yamaguchi, S.I. Kim, K.J. Park, N.K. Park, *Appl. Surf. Sci.* 310 (2014) 196–203.
- [12] S.S. Choi, M.J. Park, T. Yamaguchi, C.H. Han, S.J. Oh, S.I. Kim, J.H. Yoo, K.J. Park, Y.-S. Kim, N.K. Park, *Sens. Bio-Sens. Res.* 7 (2016) 153–161.
- [13] G.I. Taylor, D.H. Michael, *J. Fluid Mech.* 58 (1973) 625–639.
- [14] M. Lanxner, C.L. Bauer, R. Scholz, *Thin Solid Films* 150 (1987) 323–335.
- [15] K. Kanaya, S. Okayama, *J. Phys. D. Appl. Phys.* 5 (1972) 43–58.
- [16] R. Castaing, Application of Electron Probes to Local Chemical and Crystallographic Analysis (Ph.D. thesis) University of Paris, June 8 1951.
- [17] T.W. Basil, M.P. Menguc, R.R. Balance, *J. Heat Transf.* 126 (2004) 566–576.
- [18] E.H. Copland, Long Term Measurements of the Vapor Pressure of Gold in the Au-C System, NASA/CR 2009–215498, 2009.
- [19] A. Howie, *Nature* 320 (1986) 684.
- [20] E.M. Bringa, R.E. Johnson, *Phys. Rev. Lett.* 88 (2002) 165501.
- [21] T. Yokota, M. Murayama, J.M. Howe, *Phys. Rev. Lett.* 91 (2003) 265504.
- [22] J.-G. Lee, H. Mori, *Sci. Technol. Adv. Mater.* 5 (2004) 51–55.
- [23] T.J. Bullough, *Philos. Mag.* A 75 (1997) 69–85.
- [24] S. Bysakh, M. Shimojo, K. Mitsuishi, K. Furuya, *J. Vac. Sci. Technol. B* 22 (2004) 2620–2627.
- [25] N. Doraiswamy, L.D. Marks, *Surf. Sci.* 348 (1996) L67–L69.
- [26] P. Williams, *Appl. Phys. Lett.* 50 (1987) 1760.
- [27] P. Buffat, J.-P. Borel, *Phys. Rev. A* 13 (1976) 2287.
- [28] J.J. Hren, Chapter 10, Barriers to AEM: Contamination and Etching, *Introduction to Analytical Electron Microscopy*, Plenum Press, New York 1979, pp. 481–505.
- [29] R.F. Egerton, P. Li, M. Malac, *Micron* 35 (2004) 399–409.
- [30] R.F. Egerton, *Microsc. Res. Tech.* 75 (2012) 1550–1556.
- [31] L. Reimer, Chapter 10, Specimen Damage by Electron Irradiation, *Physics of Image Formation, Transmission Electron Microscopy*, Springer Series in Optical Science, fifth ed. Springer 2008, pp. 447–450.
- [32] R. Werner, M. Wanner, G. Schneider, D. Gerthsen, *Phys. Rev. B* 72 (2005) 045426.
- [33] B. Westenfelder, J.C. Meyer, J. Biskupek, S. Kurasch, F. Scholz, C.E. Krill, Iii, U. Kaiser, *Nano Lett.* 2011 5123–5127.
- [34] L.D. Marks, *Phys. Rev. Lett.* 51 (1983) 1000–1002.
- [35] K. Yoshida, A. Bright, N. Tanaka, *J. Electron Microsc.* 61 (2012) 99–103.